Nuclear reaction dynamics using loosely bound projectile ^{9}Be and associated incomplete fusion analysis

A thesis submitted in partial fulfillment of the requirements for the award of degree of

Master of Science
In
Physics

Submitted by
Shivangi Gupta
(Roll No- 301504034)

Under the supervision of
Dr. Manoj K. Sharma
(Head and Professor of Physics)
SPMS
Thapar University, Patiala

School of Physics and Materials Science (SPMS)

Thapar University,

(Formerly Thapar Institute of Engineering and Technology)

Patiala-147004, INDIA

July- 2017

I dedicate this thesis to my brother Keshav and nephew Mehul

CERTIFICATE

I hereby certify that the work which has been presented in this thesis entitled, "**Nuclear reaction dynamics using loosely bound projectile ^{9}Be and associated incomplete fusion analysis**" submitted in partial fulfillment of the requirements for the award of degree of **Master of Science** in **Physics** at **Thapar University, Patiala,** is an authentic record of my own work carried out under the supervision of **Dr. Manoj K. Sharma, Professor & Head, SPMS** and refers other researcher's work which are duly listed in reference section.

The matter embodied in this thesis has not been submitted for the award of any other degree of this or any other university.

Shivangi Gupta

Date: 1/8/2017 (Shivangi Gupta)

This is to certify that the above statement made by the candidate is correct and true to best of my knowledge.

Dr. Manoj K. Sharma
Professor and Head of Deptt.
SPMS, Thapar University
Patiala

Acknowledgement

More so than anything else, I express my deepest thanks and gratitude to the All Powerful who has been there through it all.

It is of immense pleasure to acknowledge my sincere gratitude to **Dr. Manoj K. Sharma**, my worthy supervisor, **Professor and Head of "School of Physics and Material Scienc**e." Without him this dissertation would not have been viable. His guidance helped me in all the time of research and inscribing of this dissertation. His visionary thoughts have influenced me profoundly. It is of great pleasure to work under his supervision.

My sincere thanks also go to my mentor **Ms. Neha Grover**, research scholar, for the help and valuable suggestions provided by her. I got greatly benefited from her keen scientific insight and her knack for solving seemingly intractable difficulties. Her dedication, keen interest, kindness, scholarly advice and scientific approach have enabled me to complete my thesis. I owe a debt of gratitude to all the members of the Nuclear Theory Lab for all the valuable guidance all through this effort.

Special thanks to my friends Vrinda, Mehak and Amrit for all the joy that they brought into my life and the staff at the School of Physics and Material Science for providing me a friendly atmosphere and encouraging me round the slog.

I would like to express my heart-felt gratitude to my family for their love.

I also place on record, my sense of gratitude to one and all that directly or indirectly, have lent their hand in this venture.

Date: Shivangi Gupta

Contents

List of figures

List of Tables:

Abstract

In order to study the nuclear reaction dynamics associated with $^{9}Be+ ^{89}Y$ reaction, dynamical cluster decay model (DCM) has been used. Calculations have been carried out over a broad set of center-of-mass energies varying from ($E_{c.m.}$ =18.1-29.8 MeV). A comparative analysis of complete and incomplete fusion reaction is presented for weakly bound projectile "^{9}Be". All estimations are done using quadruple choice of fragments and optimum orientation approach. In addition to this, comparison of various isotopes of technetium ($^{96, 98, 99, 100, 102, 104}Tc$) has also been studied by addressing their respective decay paths.

This dissertation is focused on following three chapters.

Chapter-1:

Chapter-1 includes the basic impression of nuclear physics including its applications and benefits to mankind. In addition to this, various mathematical models dealing with nuclear structural properties are briefly discussed here. Furthermore, nuclear reactions and their types on the basis of distinct parameters like energy, mass and compound nucleus formation etc. are explained. Besides this, a description of compound nucleus formation and its successive decay mechanisms is briefly outlined in view of dynamical evolution of heavy ion induced collisions at low energy regime.

Chapter-2:

Chapter-2 consists of the methodology used to understand reaction dynamics of ^{9}Be induced reaction(s). The Dynamical Cluster-Decay Model (DCM) is used to analyze the fragmentation behavior governed for complete fusion and incomplete fusion paths.

Chapter-3:

Chapter-3 gives an account of the analysis of the decay patterns governed via complete and incomplete amalgamation of ^{9}Be projectile with medium mass target, and consists of DCM based calculations and the results obtained/conclusions drawn after performing the analysis of concerned reaction. Calculations are done over a wide range of incident energies and DCM based results are found in decent agreement with available experimental data.

CHAPTER 1

Literature survey

1.1 Introduction:

The branch of physics associated with the study of atomic nucleus is termed as nuclear physics. The main initialization of nuclear physics is because of Becquerel's discovery of naturally occurring radioactivity in 1896. The significance of this phenomenon appeared more pronounced after two years when Pierre and Marie Curie got success in dissociation of radium (Z=88), which is a naturally occurring radioactive element. Soon after it was realized that there is influence of magnetic field on the properties of an element, as in the presence of it, some of the rays (termed α, β and γ) from the element get deflected in one direction, some in opposite direction and remaining are unaffected by the magnetic field. Afterwards, it was found that α-rays are helium nucleus (2 protons and 2 neutrons), γ-rays are just electromagnetic radiations with very short wavelength and β-rays are high energy electrons. Further, the existence of nucleus came into picture owing to Rutherford's hypothesis in 1911. Considering these discoveries and present studies on nuclear physics, it is clear that experimental and theoretical studies in nuclear physics led us to the current understanding of nucleus and have played a prominent role in the development of existing phenomena in physics.

The four elementary forces namely *the electromagnetic force*, *strong force*, *weak force* and *gravitational force* are responsible for all the phenomena taking place in the Universe. The first three mentioned forces play a very important role in the existence of nucleus. The main constituents of a nucleus are neutrons and protons where neutron is uncharged and proton has a positive charge. So, one can say that the nucleus carries its charge only because of protons. Now, the question that arises is how a nucleus can exist with only positive charge because same charges may lead to repulsions due to electromagnetic force inside the nucleus. After lots of investigations, scientists have encountered a strong interaction which is attractive and stronger than Coulomb interaction. Further, weak forces are responsible for the transformation between the nucleonic sates. The last mentioned force i.e. gravitational force is much more attractive and the main influence of this force can be observed in neutron stars. The study of these four fundamental forces is essential to understand the nuclear behavior. In various reactions, nuclear forces play a very crucial role during the collision between two nuclei and hence all reactions exhibit different nuclear properties. These nuclear properties can be extracted from the research of nuclear structure, and hence the analysis of nuclear structure is also one of the central points for better understanding of the dynamics involved.

Nuclear physics has the potential for future discoveries. A nucleus behaves like a bridge between the microscopic and the astronomical world. Further, this field is also related to other operative disciplines of research like particle physics (through fundamental interactions and symmetries) and condensed matter physics in which many body nature of the problem is involved. Also, geophysics, nuclear medicine, archaeology and tracer element systems etc. possess many benefits from nuclear physics. Thus, various applications of nuclear physics e.g. nuclear diagnostic techniques, nuclear medicine, resonance imaging, nuclear engineering etc. are extremely beneficial to mankind. There are three major aims of nuclear physics:-

1. To analyze the fundamental particles and the respective interactions between them.
2. Exploring and categorizing the nuclear properties.
3. To provide benefits to mankind or society via technological advances [1, 2].

Summarizing the above discussion, one may conclude that directly or indirectly, nuclear physics is quite advantageous to mankind. Despite all the above mentioned applications, benefits and a lot of research in nuclear physics, still there are many things that are yet to be resolved. This is primarily due to the very small size of nucleus, having radius of the order of Fermi (an order of four smaller than the dimensions of an atom).

Apart from the size of nucleus, nuclear structure is also one of the important components to comprehend. Atomic nucleus has both single particle and collective modes of excitations which make its structure more complicated. The single particle motion describes the average effect of potential on one nucleon due to all other nucleons and collective modes are related to the rotations and vibrations of all the nucleons. Therefore, to understand the complexity of this many body structure, both static and dynamic properties of nucleus need to be addressed. Various mathematical models were proposed to have an insight into its widespread properties and structural effects. Since a nucleus may consist of hundreds of nucleons, therefore, by applying some approximations we can treat it as a classical system instead of quantum-mechanical one, thus giving rise to the Liquid Drop Model (LDM) following macroscopic approach. This model was able to characterize the numerous features of nuclei such as the general behavior of binding energy for different mass numbers and the fusion-fission dynamics. However, it failed to account for the extra stability due to certain proton and neutron numbers i.e. magic numbers. Also this model did not include the effect of non-uniform distribution of nucleons because it was limited only up to macroscopic approach. Therefore, to fix these issues, rectification in macroscopic approach was done by means of Shell Model which marked out the behavior of magic numbers and described nuclear

characteristics like angular momentum, shape, magnetic moment and nuclear spectra etc. However, it remained silent about various aspects such as nuclear deformations, related orientations etc, which were further understood by Nilsson Model. Besides this, the motion of an entire nucleus including quantized rotations and vibrations, which were left undefined by Shell Model, are exercised by Collective Model. This study of rotations and vibrations by collective model is relevant to explain the coherent behavior of all the nucleons and hence useful to extract information about nuclear behavior and phenomena like magnetic rotation, super deformations etc. Further, merging of both Shell Model and Collective Model provide a route to more realistic approach known as the Unified Model. Above mentioned all mathematical models have proved to be constructive to understand the nuclear structure and related properties, and hence have become an essential part in the overall development of nuclear physics. Further, properties and structural effects of nucleus can be better understood via nuclear reactions which are explained below [2].

1.2 Nuclear Reactions:

A nuclear reaction is clearly defined as a collision taking place between two nuclei which brings out some alteration in the nuclear composition and/or the energy state of the interacting species. In a classic nuclear reaction, the incident projectile hits the target nucleus resulting into the emission of fragments. The classification of nuclear reactions can be done on the basis of various features like

1. Energy of projectile
2. Type of incident nuclei
3. Mass and types of mechanism involved etc.

On the basis of energy of the projectile involved, nuclear reactions can be classified into three types of energy range (a) low energy (b) intermediate energy and (c) high energy reactions. The **low energy reactions** occur at incident beam energy $E_{beam} \leq 15$ MeV/nucleon and significantly describe the fusion, fission, cluster decay processes and particle evaporation etc. In this energy range, we basically study nuclear properties, shapes, size, resonance, super heavy symmetries, models, reactions, dynamics, halo shapes etc. The energy range $15 < E_{beam} \leq 500$ MeV/nucleon corresponds to **intermediate energy reactions** where we study processes like multi fragmentation, particle production, nuclear flow, stopping, balance energy etc. while the reactions having $E_{beam} > 500$MeV/nucleon corresponds to **high energy**

nuclear reactions and these reactions fall under the realm of particle physics where we talk about various elementary particles such as quarks, mesons, neutrons, protons, neutrinos etc. Therefore, each one of these reactions, with their own particular framework, helps in better understanding of reaction dynamics and nuclear physics as a whole. The present work in this thesis is confined to low energy heavy ion nuclear reactions and the associated dynamical aspects. On the basis of the mechanism of the reaction involved, we can distinguish the two supreme aspects of nuclear reactions termed as compound nucleus and non-compound nucleus reactions [2].

1.2.1 Compound nucleus reactions (CN):

Reactions in which the projectile collides with the target and shares its energy among all the nucleons and forms a single excited equilibrated state, called compound nucleus (CN), are termed as compound nucleus reactions. Symbolically, we can represent this as follows:

$$a + X \rightarrow C^{*} \rightarrow Y + b$$

where C^{*} indicates the compound nucleus.

The concept of compound nucleus reactions was firstly proposed by Neil Bohr in 1936. According to him, CN reactions form a two stage process. First stage corresponds to the capture of projectile by the target nucleus with adequate amount of kinetic energy in order to prevail over the mutual electrostatic repulsions and in the latter stage; there is distribution of energy amongst all the nucleons of the composite system. Therefore, the life span of compound nucleus is sufficiently long (10^{-14}-10^{-16}s) as compared to the characteristic nuclear interaction time (10^{-21} - 10^{-22}s) and in all the degrees of freedom it is statistically equilibrated. During the formation of compound nucleus, redistribution of energy and momentum takes place uniformly among the entire system resulting into the loss of memory of formation channel. At low energies, compound nucleus reactions play a vital role in extracting productive information about the nuclear structure [2, 3].

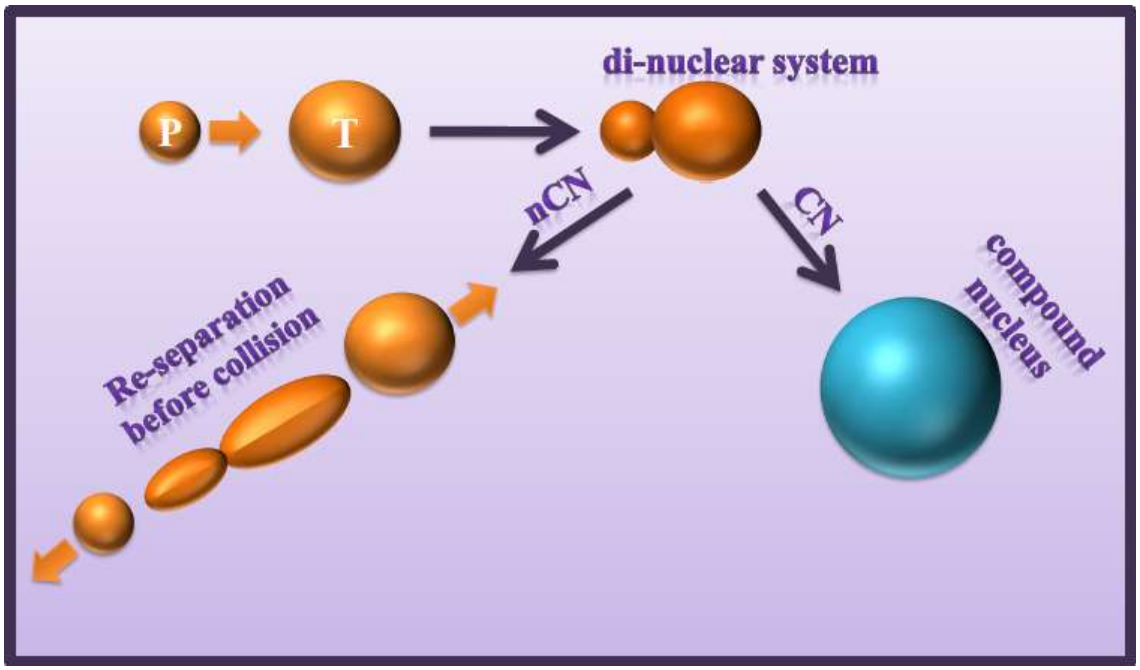

Fig.1.1. *Classification of nuclear reactions on the basis of mechanism of reaction involved as compound nucleus (CN) and non-compound nucleus (nCN) reactions [2].*

1.2.2 Non-compound nucleus reactions (nCN):

Depending upon the entrance channel, incident energy and mass asymmetry, in nCN reactions there is no evolution/production of fully equilibrated state of compound nucleus during the interaction of projectile with the target. Here the two interacting nuclei may re-separate prematurely into two fragments without forming CN. Such reactions are called non-compound nucleus reactions. The interaction time for nCN processes is much smaller than the life time of compound nucleus but sufficiently long for the transfer of mass and energy. Unlike CN, the nCN mechanism recognizes the history of its occurrence and hence it draws the entrance channel properties [2]. A broad classification of CN and nCN evolution is shown in Fig.1.1.

Table 1.1: *Tabular representation showing the comparison between compound nucleus and non-compound nucleus reactions*

Compound nucleus reactions (CN)	**Non-compound nucleus reactions (nCN)**
1. Projectile collides with the target nucleus and shares its energy among all the nucleons to form a single excited equilibrated state called compound nucleus (CN).	1. There is no production of fully equilibrated state of compound nucleus during the interaction of projectile with the target.
2. CN formation is not an immediate process and it resides inside the pocket of potential.	2. Here, the composite or di-nuclear system does not reside inside the pocket and possesses relatively smaller lifetime.
3. CN forgets its history of formation.	3. It remembers the history of its occurrence and is consequently influenced by the entrance channel.
4. Examples include complete fusion, incomplete fusion, fusion-fission, evaporation residue etc.	4. Examples include quasi fission, deep inelastic collision, fast fission etc.

In the present work, the main purpose is to study the compound nucleus reactions and therefore, to have an insight of the composite system and the evolution of CN, we need to address its formation along with various decay mechanisms. Depending upon the impact parameter for the evolution of the compound nucleus and the appropriate shape of the projectile, the reactions involving compound nucleus formation are characterized as:

1. Complete fusion (CF)
2. Incomplete fusion (ICF)

1.3 Complete fusion (CF):

Complete fusion between heavy ions can be defined as the mechanism in which the total incident beam completely fuses with the target i.e. there is complete amalgamation of all the nucleons of the projectile and the target, such that the linear momentum is entirely transferred to the target nucleus and a single excited composite system is formed inside the fission

barrier [4, 5]. In order to form CN via complete fusion reaction, the kinetic energy of the two interacting nuclei must be high enough to overcome the long range Coulomb barrier because of the mutual electrostatic repulsion between the protons, and to outdo the effect of Coulomb repulsions; the short range attractive nuclear potential brings the two nuclei fairly close to one another such that they collide with sufficient energy [6, 7]. Basically, CF is the sum of direct complete fusion (DCF) and sequential complete fusion (SCF). When the entire projectile directly amalgamates into the target nucleus without its break-up or dissociation into any other channel, the process is called *direct complete fusion* (DCF). However, if the projectile dissociates prior to the fusion into two fragments and then there is successive fusion of these fragments with the target nucleus to form CN, then the process is known as sequential complete fusion (SCF). Experimentally, it is quite difficult to make a distinction between DCF and SCF because in both cases, the compound nucleus formed is identical [4, 8].

1.4 Incomplete fusion (ICF):

When the resulting compound nucleus consists of some of the constituents or nucleons of projectile, we employ the term *incomplete fusion* (ICF). Here, the projectile is assumed to dissociate into two fragments one of which fuses with the target nucleus whereas another one is dispersed out of the interaction region with almost same velocity as that of incident ion. Therefore, in ICF there is fusion of a proportion of the projectile's mass with the target [5, 9] and the other part of projectile is emitted as a spectator in order to release excess driving angular momentum. Hence, only fractional exchange of angular momentum takes place in ICF. The compound nucleus formed in this case has comparatively less charge, mass and excitation energy in contrast to the CN formed in complete fusion reactions. Generally, in these processes the collision trajectories have a higher value of impact parameter and thus the centrifugal potential predominates over the attractive nuclear potential due to which CF is hindered leading to ICF [2, 10]. Therefore, the most common features of ICF can be understood as follows:

1. In ICF, the particles in the exit channel possess forward peaked angular spread.
2. The outgoing particles have an energy spectrum which acquires peaks at beam velocity.
3. Short-range components are seen to be observed due to the recoil range distribution of heavy residues, indicating partial momentum transfer.

It has also been observed that as the projectile energy increases, ICF becomes more and more prominent and CF steadily gives way to ICF at relatively higher beam energies at finite values of impact parameter [11]. ICF process is also known as massive transfer, breakup fusion, pre-compound or prompt emission of particles. A pictorial distribution of ICF dynamics is given below in Fig.1.2.

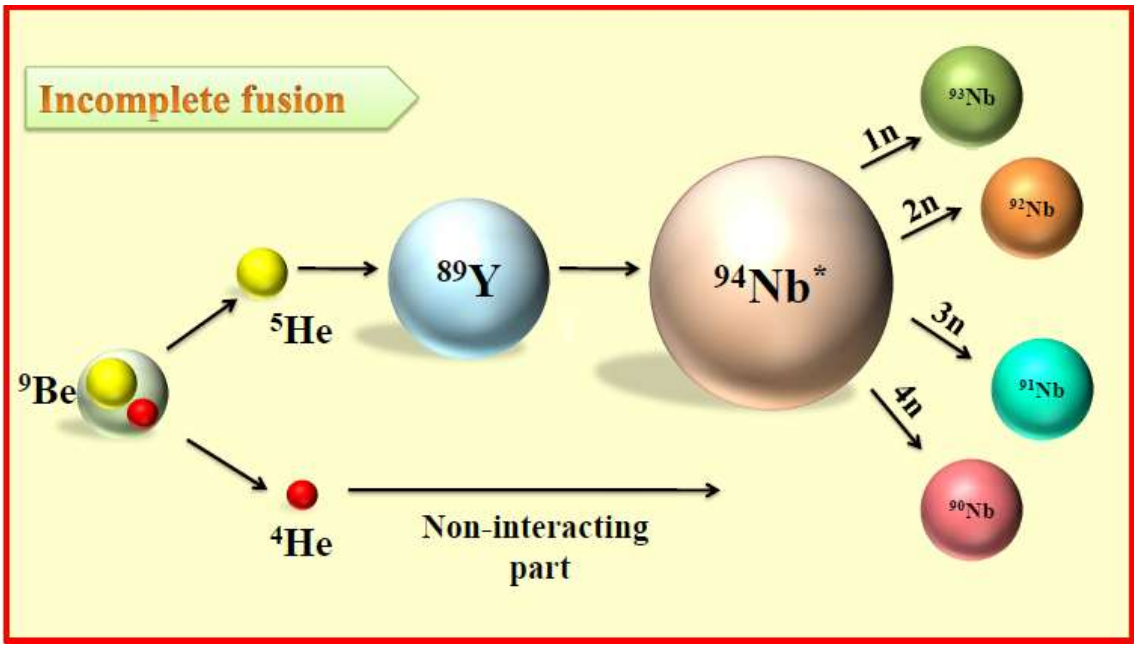

Fig.1.2. *Pictorial representation of incomplete fusion (ICF) forming $^{94}Nb^{*}$ through $^{9}Be + {}^{89}Y$ as break-up channel [12].*

1.5 Decay of Compound nucleus:

A compound nucleus may decay via single or multiple modes, exhibiting a variety of decay mechanisms. Since a compound nucleus forgets the history of its formation, therefore, its decay does not depend upon the incident channel and hence it can disintegrate through various processes by emitting light particles, intermediate mass fragments, heavy mass fragments and symmetric/asymmetric fission fragments [13]. The decay of compound nucleus can be through any of the above mentioned decay modes according to its mass, as follows:

For light mass compound systems, i.e. for A_{CN} ~ 40-80, light particle emission (LPs; $Z_2 \leq 2$ and $A_2 \leq 4$) is the major decay mode along with very small contribution of intermediate mass fragments (IMFs; $2 \leq Z_2 \leq 10$ and $5 \leq A_2 \leq 20$).

For intermediate mass nuclear systems, i.e. for A_{CN} ~ 80-200, there is competition between LPs and fission fragments [14, 15].

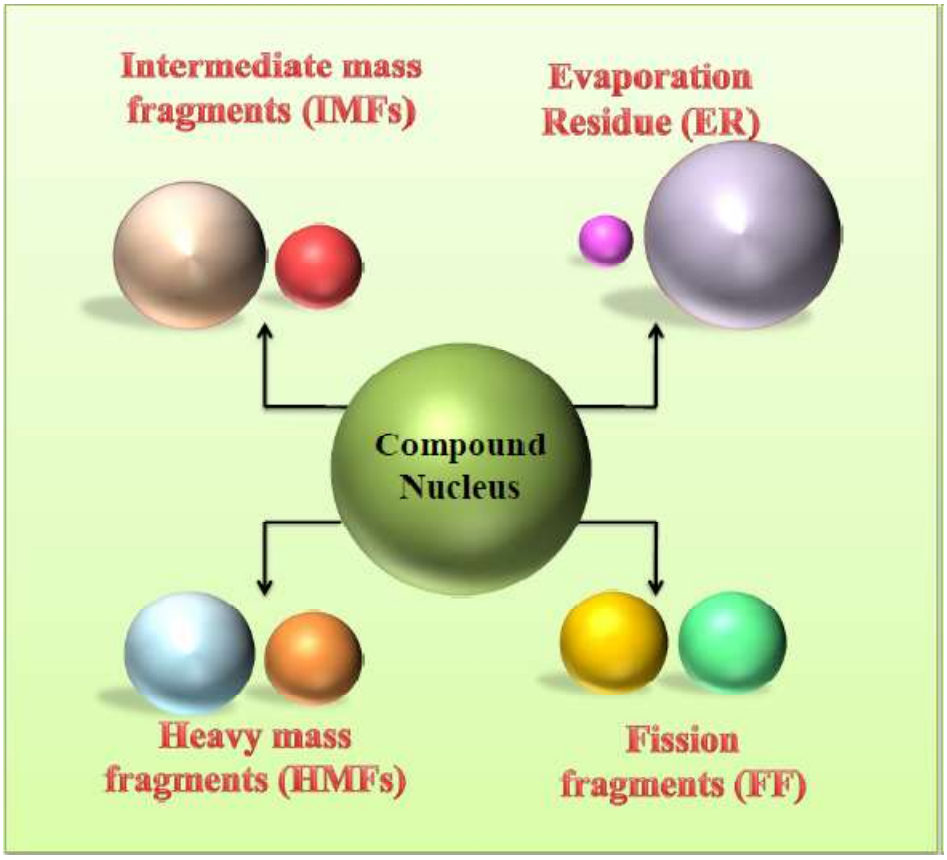

Fig.1.3. *Various decay modes through compound nucleus (CN).*

For heavy mass compound systems, i.e. for $A_{CN} \geq 200$, due to the existence of large number of protons, Coulombic repulsions rapidly increase and as a result symmetric or asymmetric fission fragments may form. However, in case of high degrees of asymmetry between the fragments, emission of heavy mass fragments (HMFs; $20 \leq A_2 \leq A_{CN}/2$) may also take place. A brief description of above mentioned decay paths is shown in Fig.1.3.

1.6 Importance of the present work:

The present work is solely focused on the nuclear reaction dynamics exhibited by weakly bound projectile ^{9}Be. Weakly bound nuclei are basically some of the rare nuclei lying away from the line of stability which exhibit modified forms of nuclear matter and unprecedented exotic behavior. This exotic behavior primarily refers to their strange/peculiar kind of decay

modes like proton radioactivity and β-delayed particle emission etc. which are not observed in the nuclei lying near stability region. The inner structure of such nuclei deviates from the traditional shape and structure of nuclei and have small separation energy of the order of 1-2 MeV. ^{11}Li was the first weakly bound isotope discovered in 1985 [16]. The certain properties which make a weakly bound nucleus an object of concern include; its low breakup threshold which is because of its less binding energy per nucleon, few unbound excited states, larger rms radii as compared to its value estimated from systematics ($R = r_oA^{1/3}$), greater transfer probability etc. [12]. Out of all the weakly bound nuclei locating near or far from the stability line, special attention has been given to halo nuclei. This halo feature is exhibited by those weakly bound nuclei in which the last one or two valence nucleons are very loosely bound to the nucleus and hence these nucleons (neutrons or protons) decouple from the inert core containing all the other nucleons. The loosely bound valence nucleons circulate around the core in an orbit which possesses much higher radius than that of the core. This accounts for very large interaction cross sections for weakly bound nuclei like helium, lithium etc. [4, 17]. Some of the fundamental properties that are necessary for nuclei to exhibit halo behavior include low dissociation energy of the valence nucleon, decoupling from the core and a wave function acquiring relatively low angular momentum state. The halo structure has been proved for various cases like ^{11}Li, ^{14}Be, ^{11}Be, ^{19}C, ^{14}B, ^{15}C and ^{8}B etc. with ^{11}Li being the most famous halo nucleus.

Fusion reactions induced by loosely bound projectiles are very fascinating owing to their importance in astrophysical reactions as they lend a hand in understanding the nucleosynthesis process [18, 19]. When a weakly bound projectile is incident on the target nucleus, it may break into fragments and therefore, the reactions induced with weakly bound projectiles help us to distinguish CF and ICF because of the emission of distinct type of evaporation residues in the two reactions. Also, there are many experimental advantages of break-up measurements of reactions induced with weakly bound nuclei as they largely break into charged fragments that can be detected with relatively easier approach than neutrons [20]. The considerably high beam intensity of stable weakly bound nuclei as compared to radioactive beams makes them an important and interesting subject to examine and hence to investigate the influence of break-up processes in heavy ion reactions [21]. Hence, a versatile theory of incomplete fusion (ICF) can be developed which may provide assistance in studying the accumulation of high spin states by means of fusion processes.

Considering the significance of weakly bound projectiles, the investigation regarding the breakup effects of ^{9}Be on fusion is elaborated in the present work by exploring the fragmentation paths of CF and ICF channels. ^{9}Be is a strongly deformed and stable weakly bound nucleus which possess an α+ *x* cluster structure, and the breakup of ^{9}Be into two or more fragments has low threshold energies. Owing to these distinctive properties, it is increasingly used as a projectile nowadays for the study of nuclear structure and reaction dynamics [22]. Firstly an analysis of incomplete fusion has been carried out for reaction $^{9}Be + {}^{89}Y \rightarrow {}^{98}Tc^{*}$ induced with weakly bound projectile. This study is done over a wide range of incident energies. In addition to ICF study, a comparative analysis with corresponding CF mechanism is worked out and subsequently the decay profile of various isotopes of technetium (Tc) has also been addressed using weakly bound projectiles. The calculations are done using the dynamical cluster decay model (DCM), which is briefly discussed in Chapter 2. The calculations, results and conclusions drawn are finally illustrated in Chapter 3.

References:

[1] Kenneth S. Krane**,** Introductory Nuclear Physics, Pg. No. 13.

[2] http://dspace.thapar.edu:8080/jspui/bitstream/10266/3779/1/Gurvinder_thesis_upload.pdf.

[3]S. N. Ghoshal Phys. Rev.**80**, 6 (1950).

[4]L.F. Canto, P.R.S. Gomes, R. Donangelo, M.S. Hussein, Phys. Rep. **424** (2006) 1 – 111.

[5]Manoj Kumar Sharma, Unnati, B.K. Sharma *et al.,* Phys. Rev. C **70**, 044606 (2004).

[6] M. Dasgupta, D. J. Hinde, R. D. Butt *et al.,* Phys. Rev. Lett. **82**, 7 (1999).

[7]Manjeet Singh, Sukhvinder, Rajesh Kharab, Nucl. Phys.A**897**, 179–197(2013).

[8] A Mukherjeeand M K Pradhan, Pramana – J. Phys.**75**, No. 1 (2010).

[9] L.F. Canto, P.R.S. Gomes, R. Donangelo, J. Lubian, M.S. Hussein, Phys. Rep. **596,** 1–86 (2015) .

[10] L. F. Canto, R. Donangelo, and Lia M. de Matos Phys. Rev. C **58**, 2 (1998).

[11] F. K. Amanuel,B. Zelalem,A. K. Chaubey*et al.,*Phys. Rev. C **84**, 024614 (2011).

[12]C. S. Palshetkar, S. Santra*et al.*, Phys. Rev. C **82,** 044608 (2010).

[13] B. Ivle, Phys. Rev. C **87**, 034619 (2013).

[14]BirBikramSingh,Manoj K. Sharmaand Raj K. Gupta, Phys. Rev. C 77, 054613 (2008).

[15] M. Kumar, R. Kumar and M. K. Sharma, Phys. Rev. C **85**, 014609 (2012).

[16]ChhandaSamanta,Pramana – J. Phys.**57**, No's 2 & 3 (2001).

[17] J. Al-Khalili, An Introduction to Halo Nuclei, Lect. Notes Phys. **651**, 77–112 (2004).

[18]Yu. E. Penionzhkevich, Physics of Atomic Nuclei **73**, 8 (2010).

[19]C.A. Bertulani, X Latin American Symposium on Nuclear Physics and Applications (X LASNPA),1-6 December 2013Montevideo, Uruguay.

[20] T. Ishii, M. Itohb*et al.*, Nuclear Instruments and Methods in Physics Research A **395**, 210 (1997).

[21]K.P.Santhosh,V.BobbyJose, Nucl. Phys. A **922** (2014) 191–199.

[22]V. V. Parkar,R. Palit,Sushil K. Sharma*et al.*, Phys. Rev. C **82,** 054601 (2010).

CHAPTER 2:

Methodology

The Dynamical Cluster Decay Model (DCM)

The Dynamical Cluster-Decay Model (DCM) [1-7] is basically an explicative edition in the preformed cluster model (PCM) [8-11] and both these models have in turn originated from the Quantum Mechanical Fragmentation Theory (QMFT) [12-13].

DCM is explicitly studied to address the various decay mechanisms of compound nucleus (CN) and non- compound nucleus reactions (nCN) by considering the role of components like excitation energy, temperature, angular momentum, deformations/orientations etc. of the decaying fragments. The total cross sections may have contribution from evaporation residues, intermediate mass fragments (IMFs), heavy mass fragments (HMFs) and fission fragments, and the calculations are carried out in terms of mass asymmetry $\{\eta_A = (A_1\text{-}A_2) / (A_1+A_2)\}$ of fragments in the outgoing channel. The DCM based decay cross sections are extracted as function of preformation probability P_0 and barrier penetration probability P by using the partial wave analysis as:

$$\sigma = \frac{\pi}{k^2} \sum_{l=0}^{l_{max}} (2l+1)\, P_0 P \tag{1}$$

where k is written as $k = \sqrt{\frac{2\mu E_{c.m.}}{\hbar^2}}$ with reduced mass μ represented as

$$\mu = \left[\frac{A_1 A_2}{(A_1 + A_2)}\right] m = \frac{1}{4} Am(1-\eta^2)$$

here, m represents the nucleon mass and ℓ_{max} denotes the maximum angular momentum value which is set corresponding to the point where the light particle cross sections become imperceptible ($\sigma_{LP} \rightarrow 0$).

Fundamentally, DCM can be viewed as a two-step model where the former step involves calculating the value of preformation factor (P_0) of the decaying fragments which refers to the η (asymmetry) motion and the latter step involves the barrier penetration of the fragments (tunneling) which indicates the R motion. The calculations are done using decoupled motion approach independently for η and R dependence [13].

Note that the components P_0 and P in equation (1) depend upon ℓ and T of selected reaction along with deformations and orientations of the decaying fragments.

For η -motion, i.e. in order to calculate the preformation probability P_0, the stationary Schrödinger equation needs to be solved in η-coordinates at a particular value of relative separation distance R, and the equation is as follows:

$$\left\{-\frac{\hbar^2}{2\sqrt{B_{\eta\eta}}}\frac{\partial}{\partial\eta}\frac{1}{\sqrt{B_{\eta\eta}}}\frac{\partial}{\partial\eta}+V_R(\eta,T)\right\}\psi^{\nu}(\eta)=E^{\nu}\psi^{\nu}(\eta) \tag{2}$$

With ν = 0, 1, 2, 3…. where ν = 0 refers to ground state and ν = 1, 2, 3…. attributes to other excited state solutions for greater values of ν and mass parameter $B_{\eta\eta}$ is the smooth classical hydro-dynamical mass [14] representing the kinetic energy part.

$V_R(\eta,T)$ in equation (2) is termed as fragmentation potential and is given by:

$$\begin{aligned}V_R(\eta,T)=&\sum_{i=1}^{2}\left[V_{LDM}(A_i,Z_i,T)\right]+\sum_{i=1}^{2}\left[\delta U_i\right]\exp(-T^2/T_0^2)+V_c(R,Z_i,\beta_{\lambda i},\theta_i,T)\\&+V_P(R,A_i,\beta_{\lambda i},\theta_i,T)+V_\ell(R,A_i,\beta_{\lambda i},\theta_i,T)\end{aligned} \tag{3}$$

where,

$$B=V_{LDM}(T=0)+\delta U$$

represents the binding energy contribution [15, 16, 17]. The terms V_C, V_P and V_ℓ in equation (3) represents the temperature dependent Coulomb, Proximity and Centrifugal Potential and can be expressed through following equations-

(i) <u>Coulomb Potential (V_C):</u>

$$\begin{aligned}&V_c(R,Z_i,\beta_{\lambda i},\theta_i,T)\\&=\frac{Z_1Z_2e^2}{R(T)}+3Z_1Z_2e^2\\&\times\sum_{\lambda,i=1,2}\frac{R_i^{\lambda}(\alpha_i,T)}{(2\lambda+1)R(T)^{\lambda+1}}Y_\lambda^{(0)}(\theta_i)\left[\beta_{\lambda i}+\frac{4}{7}\beta_{\lambda i}^2Y_\lambda^{(0)}(\theta_i)\right]\end{aligned} \tag{4}$$

(ii) <u>Proximity Potential (V_P):</u>

$$V_P(s_o(T))=4\pi\bar{R}(T)\gamma b(T)\phi(s_o,(T)) \tag{5}$$

where $\phi(s_o,T)$ is universal function independent of shape and geometry and $\bar{R}(T)$ represents the mean curvature radius of reaction partners. The universal function reads as

$$\phi(s_o,T)=\begin{cases}-\frac{1}{2}(s_o(T)-2.54)^2-0.0852(s_o(T)-2.54)^3 & s_o(T)\le 1.2511\\ -3.437\exp(-s_o(T)/0.75) & s_o(T)\ge 1.2511\end{cases} \quad (6)$$

and the specific nuclear surface tension γ is given by:

$$\gamma = 0.9517\left[1-1.7826\left(\frac{N-Z}{A}\right)^2\right]\text{MeV fm}^{-2} \quad (7)$$

with surface width

$$b(T)=0.99(1+0.009T^2) \quad (8)$$

(iii)<u>Centrifugal Potential (V_ℓ):</u>

The centrifugal potential containing the angular momentum effects is given by:

$$V_\ell(T)=\frac{\hbar^2\ell(\ell+1)}{2I(T)} \quad (9)$$

where I(T) is moment of inertia which can be either sticking (I_S) or non-sticking (I_{NS}). For sticking limit of moment of inertia, separation between two nuclei R< 2 fm and is given by:

$$I(T)=I_S(T)=\mu R_a^2+\frac{2}{5}mA_1R_1^2+\frac{2}{5}mA_2R_2^2 \quad (10)$$

Now the solution of equation (2) represents the preformation probability and is given by-

$$P_0=(\frac{2}{A})\sqrt{B_{\eta\eta}}\;|\;\Psi[\eta(A_i)]\;|^2 \quad (11)$$

with (i =1, 2). Also, the ground state solution $\psi(\eta)$ is $\psi^{\nu=0}(\eta)$.

In addition to P_0, penetrability also serves as an important input towards the cross-sections. Thus, the expression for P calculated using WKB approximation is given by:-

$$P=\exp[-\tfrac{2}{\hbar}\textstyle\int_{R_a}^{R_b}\{2\mu[V(R)-Q_{eff}]\}^{1/2}\,dR] \quad (12)$$

The first turning point R_a in the above equation for the decay of a hot compound nucleus can be written as:

$$R_a=R_t(\eta)+\Delta R=R_i(\alpha_i,T)+\Delta R(T)$$

where Δ R is the relative separation distance which assimilates the neck formation effects[18, 19]. The radius vector can be written as:

$$R_i(\alpha_i, T) = R_{0i}(T)[1 + \sum_{\lambda i} Y_{\lambda}^{(0)}(\alpha_i)]$$

Here, the magnitude of R assimilates the effects of both neck formation and deformations of the two fragments to a good extent. The temperature dependence in radii R_{0i} is given as [20].

$$R_{0i} = [1.28A_i^{1/3} - 0.76 + 0.8A_i^{-1/3}](1 + 0.0007T^2) \quad (13)$$

Q_{eff} in equation (12) can be expressed in terms of binding energies of fragments in emission channel as follows:

$$Q_{eff}(T) = B(T) - [B_1(T = 0) + B_2(T = 0)] = \text{TKE (T)} = V(R_a) \quad (14)$$

The excitation energy of compound nucleus can be written in terms of temperature as:

$$E_{CN}^{*} = \left(\frac{A}{9}\right)T^2 - T \quad (15)$$

In order to calculate the energy of ICF component, we have applied the necessary and appropriate corrections in the beam energy in reference to [21].

Further, CF and ICF events can be disentangled on the grounds of degree of linear momentum transfer (LMT) from the incident projectile to the target. As far as complete fusion is concerned, the compound nucleus accumulates the whole nucleonic degrees of freedom of the projectile. On the other hand, in ICF processes the formation of compound nucleus occurs due to partial transfer of linear momentum from the incident beam.

Therefore, by drawing an idea about the terminology adopted to estimate the decay cross-sections for heavy ion induced reactions, present study is carried out for reaction in which weakly bound projectile ^{9}Be is bombarded on target nucleus ^{89}Y. In referred experimental data [22], it has been observed that the most dominant decay channel is evaporation residue (ER). Hence, we have confined ourselves to ER analysis only and the results obtained/ conclusions drawn are precisely outlined in the succeeding chapter.

References

[1] R.K. Gupta, M. Balasubramaniam, R. Kumar, D. Singh, C. Beck and W. Greiner, Phys. Rev. C **71**, 014601 (2005).

[2] R.K. Gupta, M. Balasubramaniam, R. Kumar, D. Singh, S. K. Arun and W. Greiner, J. Phys. G: Nucl. Part. Phys. **32**, 345 (2006).

[3]ManpreetKaur,BirBikramSingh,S. K. Patra,and Raj K. Gupta, Phys. Rev. C **95,**014611 (2017).

[4]GurvinderKaur,NehaGrover,KirandeepSandhu,ManojK.Sharma, Nucl. Phys.A **927,** 232–248 (2014).

[5]Neha Grover, GurvinderKaur, and Manoj K. Sharma, Phys. Rev. C **93,** 014603 (2016).

[6]NehaGrover, IshitaSharma, GurvinderKaur, Manoj K.Sharma, Nucl. Phys.A**959,**10-26(2017).

[7]Satish Kumar and Raj K. Gupta, Phys. Rev. C **55,** 218 (1997).

[8]Raj Kumar,KirandeepSandhu,Manoj K. Sharma,and Raj K. Gupta, Phys. Rev. C **87,**054610 (2013).

[9]GudveenSawhney, Manoj K. Sharma and Raj K. Gupta, Phys. Rev. C **83,**064610 (2011).

[10]Raj Kumarand Manoj K. Sharma, Phys. Rev. C **85,**054612 (2012).

[11]Satish Kumar and Raj K. Gupta, Phys. Rev. C **55,**054612 (2012).

[12] J. Maruhn and W. Greiner, Phys. Rev. Lett. **32**, 548 (1974).

[13] R.K. Gupta, W. Scheid, and W. Greiner, Phys. Rev. Lett. **35**, 353 (1975).

[14] H. Kroger and W. Scheid, J. Phys. G Nucl. Phys. **6**, L85 (1980).

[15] N.J. Davidson, S.S. Hsiao, J. Markram, H.G. Miller, and Y. Tsang, Nucl. Phys.A**570**, 61C (1994).

[16] G. Audi and A.H. Wapstra, Nucl. Phys.A**595**, 4 (1995).

[17] W. Myers and W.J. Swiatecki, Nucl. Phys.A**81**, 1 (1966).

[18] S. Kumar and R.K. Gupta, Phys. Rev. C **55**, 218 (1997).

[19] R. K. Gupta, S. Kumar, and W. Scheid, Int. J. Mod.Phys. E **6**, 259 (1997).

[20]G. Royer and J. Migner, J. Phy. G **18**, 1781 (1992), and earlier references therein.

[21] G. Kaur and M. K. Sharma, Nucl. Phys.A**884**, 36, (2012).

[22]C. S. Palshetkar, S. Santra*et al.*, Phys. Rev. C **82,** 044608 (2010).

Chapter-3

Results and Discussions

Due to availability of radioactive beams of nuclei possessing weakly bound nature, tremendous amount of experimental work has been done in the past few years to study the reaction dynamics induced with weakly bound and halo nuclei. According to literature, it has been observed that complete fusion cross sections get enhanced at sub-barrier energies in tightly bound induced reactions. However, there are assumptions that this enhancement in cross sections may be replaced with suppression in loosely bound induced reactions [1]. Now, weakly bound nuclei can be classified into stable and unstable weakly and in present work, study is mainly focused on stable weakly bound (^{9}Be) induced reaction. When a stable weakly bound projectile fuses with massive targets, it has been observed that at above-barrier energies, CF cross sections are suppressed in contrast to light mass targets [2]. Therefore, to have an insight of the nuclear dynamics shown by loosely bound systems, an attempt has been made to address the decay mechanism involved in the fusion of ^{9}Be as a projectile with neutron magic target nucleus ^{89}Y (N=50) as per the experimental data [2]. In the frame of dynamical cluster-decay model (DCM) [3, 9], the decay study has been carried out for the compound nucleus ^{98}Tc* (intermediate mass region) formed via ^{9}Be + ^{89}Y reaction. The calculations are performed at near-barrier energies varying from $E_{c.m}$=17.7 - 29.8 MeV (equivalently T= 1.622 - 1.942 MeV) and the contribution of decay mode at all energies is predominantly governed by evaporation residues (neutron cross sections *x*n; *x*=2–4) for CF. According to experimental data there is suppression in CF cross-sections due to breakup of the loosely bound "^{9}Be" projectile which results into incomplete fusion process. Therefore, the contribution from both CF and ICF processes has been analyzed via DCM calculations. It's worth pointing out the fact that the calculations have been carried out using the neck-length parameter ΔR, which is the unique parameter of DCM. Additionally, all the calculations are done by choosing deformed choice of fragments.

According to the referred data [2], the CF cross sections are suppressed by (20 ± 5)% for ^{9}Be+ ^{89}Y system which further results into incomplete fusion process observed due to the breakup of ^{9}Be. The two most favorable charged fragmentation channels for ^{9}Be are: [10]

$$^{9}\text{Be} \rightarrow {}^{1}\text{n} + {}^{4}\text{He} + {}^{4}\text{He} \quad (1)$$

$$^{9}\text{Be} \rightarrow {}^{4}\text{He} + {}^{5}\text{He} \quad (2)$$

Thus, there are three possibilities for incomplete fusion process such as-

$$^{1}\text{n} + {}^{89}\text{Y} \rightarrow {}^{90}\text{Y} \rightarrow A_1 + A_2 \quad (3)$$

$$^{4}\text{He} + {}^{89}\text{Y} \rightarrow {}^{93}\text{Nb} \rightarrow A_1 + A_2 \quad (4)$$

$$^{5}\text{He} + {}^{89}\text{Y} \rightarrow {}^{94}\text{Nb} \rightarrow A_1 + A_2 \quad (5)$$

Here an effort has been made to analyze the incomplete fusion contribution of above mentioned channels using dynamical cluster decay model. In the first place, a comparison of these three reaction channels for ICF (β_{2i}-deformed) is shown in Fig.3.1 through (a) fragmentation potential and (b) preformation probability at the lowest incident energy E_{beam}= 19.9 MeV of ^{9}Be (initial beam) which is further corrected for each channel i.e. ^{5}He + ^{89}Y → ^{94}Nb, ^{4}He + ^{89}Y → ^{93}Nb and ^{1}n+ ^{89}Y→ ^{90}Y as per reference [2]. It is assumed that energy of incident beam is distributed equally among all contributing nucleons and the ICF channel center-of-mass energies for ^{5}He, ^{4}He and ^{1}n respectively read as 10.46 MeV, 8.45 MeV and 2.18 MeV. Fig.3.1 represents the relative behavior of three reaction channels which help us to identify the one contributing most towards ICF contribution. Before proceeding, it is again emphasized that the calculations for ICF are carried out by exercising the appropriate and required energy corrections as per [2].

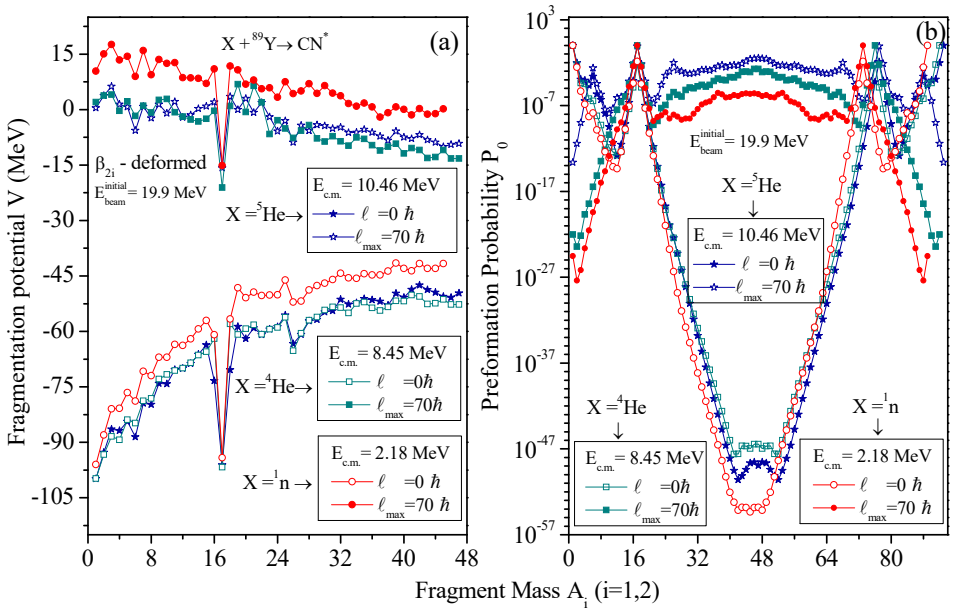

Fig.3.1. *Comparison of three different ICF reaction channels in terms of (a) fragmentation potential and (b) preformation probability with respect to fragment mass for β_{2i} deformed choice.*

The fragmentation potential ($V(A_2)$), minimized in mass-coordinate (η_A), is an input of Schrödinger wave equation, the solution of which gives us the preformation probability (P_0). Both fragmentation potential and preformation probability are plotted as a function of fragment mass represented in Fig.3.1(a) and Fig.3.1(b) respectively at ℓ=0 and ℓ=ℓ_{max}, where

ℓ_{max} is decided at a point at which the evaporation residue cross sections become negligible i.e. $\sigma_{ER} \rightarrow 0$. From the Fig.3.1(a), one can see that the overall structural behavior of potential energy surfaces (PES) remains similar for all the three reaction channels. However, the magnitude of fragmentation potential is maximum for neutron-induced reaction and for reactions having projectile ^{4}He and ^{5}He, it is almost overlapping with each other. It is important to mention here that the minima in fragmentation potential in DCM based calculations is analogous to maxima in preformation probability, which ultimately sets for the higher magnitude of cross sections for that fragment. The dip at ^{17}B is just because of the large decrement in the proximity potential probably due to inappropriate deformation of this fragment [11]. To further investigate the comparative fragmentation of ICF channels, the preformation probability (P_0) as a function of fragment mass A_i (i=1, 2) is expressed in Fig.3.1(b) where one can clearly see the broad symmetric fission distribution exhibited by all the reaction channels. The figure clearly shows that at $\ell=\ell_{max}$, probability of ER contribution is highest for ^{5}He induced reaction followed by ^{4}He and ^{1}n induced ones. Whereas at $\ell=0\hbar$, P_0 for ER is same for all reaction channels. As expected, contribution of ER is more prominent at $\ell=0\hbar$ and hence lower ℓ states contribute most towards ER cross sections.

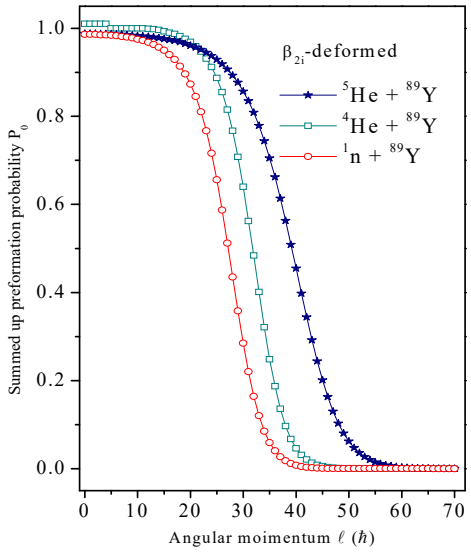

Fig.3.2. *Summed-up preformation probability (P_0) of evaporation residues through different reactions channels for ICF as a function of angular momentum ℓ at lowest initial beam E_{beam}= 19.9 MeV of ^{9}Be which is further corrected for each channel.*

At $\ell=\ell_{max}$, the probability of fission fragments is maximum for ^{5}He induced channel followed by ^{4}He and ^{1}n channel. As evident from overlapping of fragmentation potential for ^{5}He and ^{4}He channel and almost similar contribution of ER component at $\ell=0\hbar$ for all ICF cases, it becomes difficult to identify the most contributing channel in the successive break-up of ^{9}Be induced reaction regarding the prominent ICF among chosen cases. Both these figures (Fig.3.1(a),(b)) are not giving a clear picture that which reaction is more suitable as incomplete fusion channel. Therefore, the summed-up preformation probability for the dominant region i.e. evaporation residue is plotted as a function of angular momentum shown in Fig.3.2 where the preformation probability of ER through all three channels is almost same up to $\ell= 20\hbar$. However, a significant shift is seen in the variation of P_0 at $\ell > 20\hbar$ and we can clearly see that summed-up P_0 of formation of ER is maximum for ^{5}He + ^{89}Y reaction and minimum for neutron induced break-up channel for most of the partial wave region and at large values of angular momentum, P_0 becomes almost negligible for all the reaction modes. Consequently, the preformation analysis suggests that ^{5}He+^{89}Y may be chosen as best/suitable reaction channel for further investigation of ICF. In view of this, further ICF calculations are done for ^{5}He channel only.

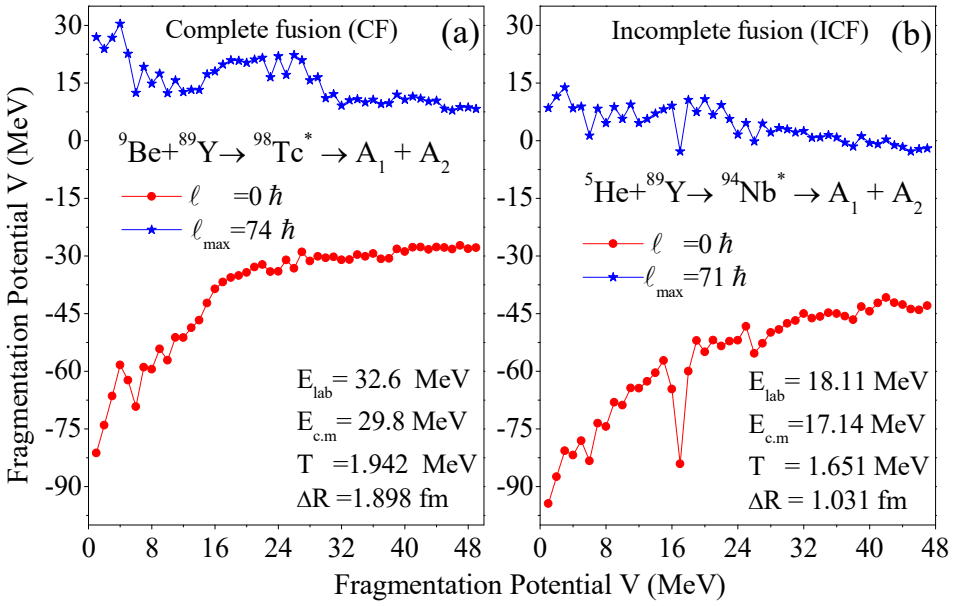

Fig.3.3. *Comparison of (a) CF and (b) ICF based fragmentation potential with respect to fragment mass (A_2) for β_{2i}- deformed choice.*

Now, in order to do a comparative study of complete and incomplete fusion, the fragmentation potential for CF and ICF (β_{2i}-deformed) are plotted as a function of fragment mass at highest incident energy in Fig.3.3. From the figure, one can see that the structural behavior of potential energy surfaces (PES) gets modified as one goes from CF to ICF channel and the magnitude becomes much lower for the ICF path. Also the neck length parameter 'ΔR' is small for ICF as compared to CF. It may be because of the small size of incident projectile. To further investigate the distinctness of CF and ICF, preformation probability (P_0) as a function of fragment mass A_i (i=1,2) is explored. Fig.3.4 shows the preformation probability for (a) complete and (b) incomplete fusion at extreme angular momentum values. It is clearly depicted from the figure that symmetric structure is exhibited by both CF and ICF. Also, the magnitude of P_0 at $\ell=\ell_{max}$ is almost same for both processes. However, the probability of formation of IMFs through ICF seems to be enhanced at maximum angular momentum.

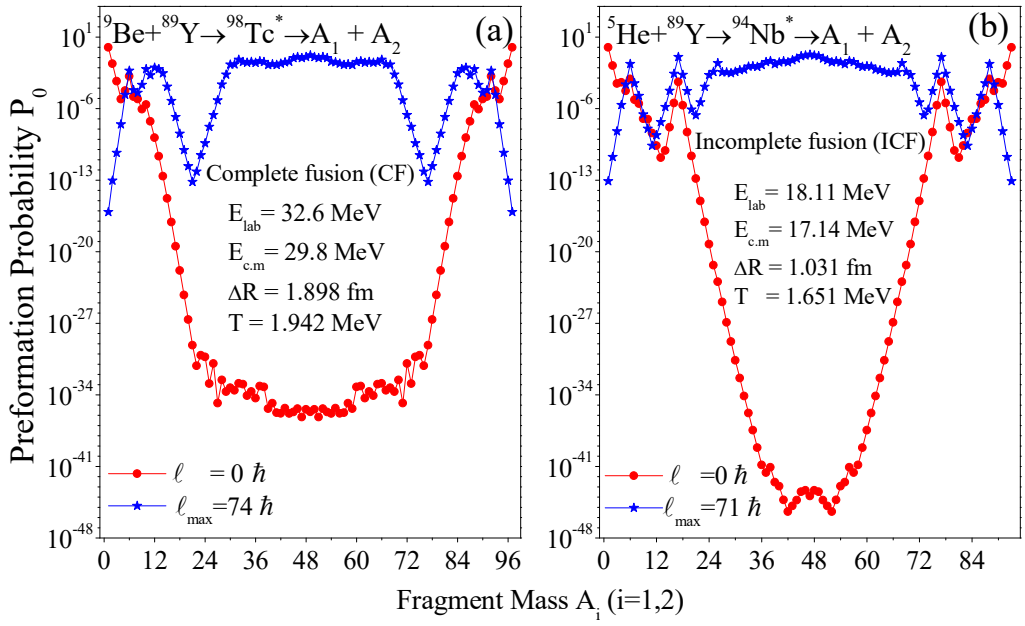

Fig.3.4. *Comparison of (a) CF and (b) ICF based preformation probability (P_0) with respect to fragment mass A_i (i=1, 2) for β_{2i}-deformed choice.*

Now, the cross sections in DCM are addressed employing the unique parameter of DCM namely the neck length parameter. The neck length parameter (ΔR) is plotted as a function of center-of-mass energy ($E_{c.m.}$) in Fig.3.5, where ΔR for complete fusion path is presented

in Fig.3.5 (a) and 3.5(b) exhibit the neck behavior for incomplete fusion process. From Fig.3.5(a) one can clearly see that with rise in center-of-mass energy, ΔR increases for CF i.e. at the highest energy ($E_{c.m.}$=29.8 MeV) ΔR is much larger as compared to its value at the lowest energy ($E_{c.m.}$= 18.1 MeV). However, in case of ICF, the magnitude of ΔR is much lower in comparison to CF. Here, also the magnitude of ΔR increases with increase in incident energy but at much slower pace than that for CF process.

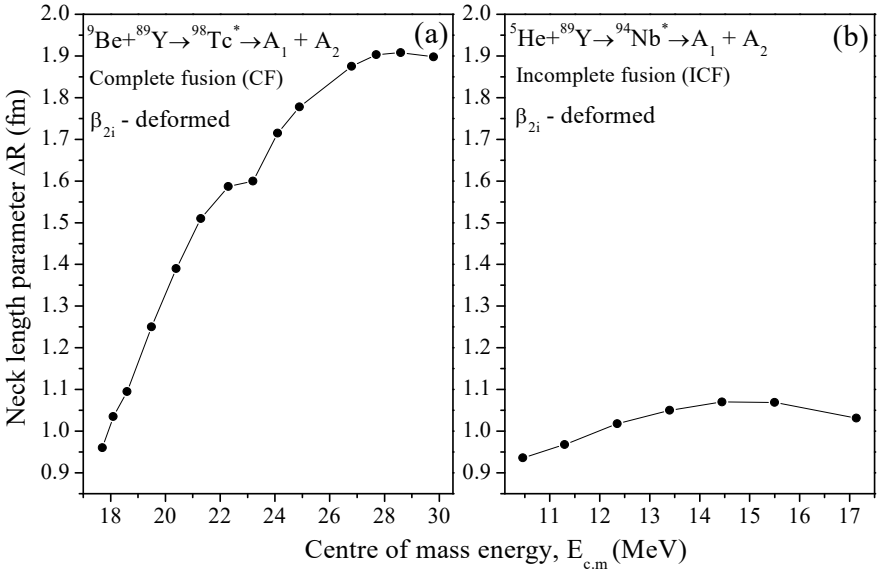

Fig.3.5. *Dependence of neck length parameter (ΔR) on center-of-mass energy ($E_{c.m.}$) for (a) CF and (b) ICF*

This inclusion of neck length parameter leads to corresponding barrier modification which is an in-built property of DCM and has a straight dependence on the choice of neck length parameter ΔR. The variation of ΔV_B with center-of-mass energy is elaborated in Fig.3.6. Moreover, it is important to state that ΔV_B is plotted for most dominant decaying fragment (shown in Fig.3.6) for both CF and ICF components.

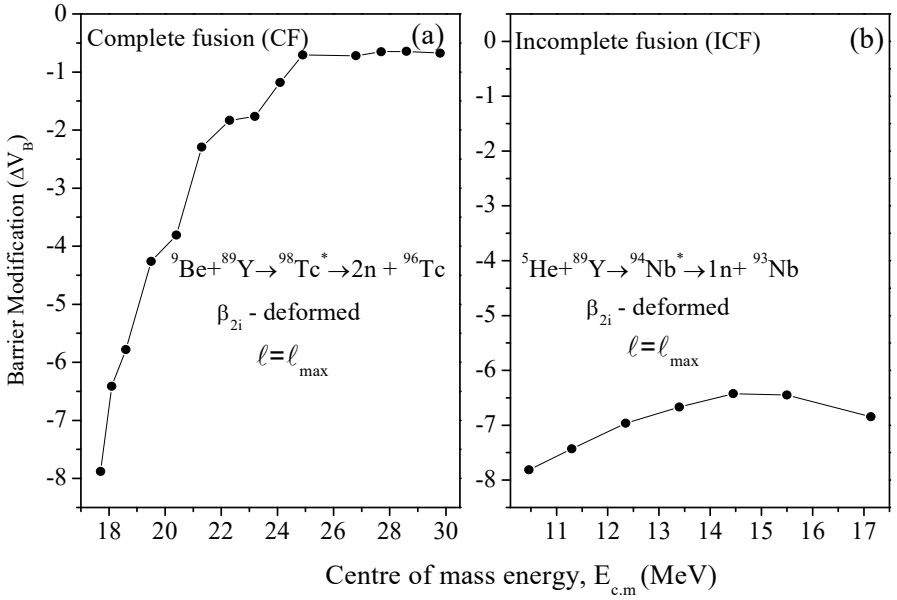

Fig.3.6. *Dependence of barrier lowering parameter ΔV_B on center-of-mass energy ($E_{c.m.}$) for (a) CF and (b) ICF at $\ell=\ell_{max.}$*

From Fig.3.6(a), it is observed that the magnitude of ΔV_B (non-zero negative number at all energies) is highest at the lowest energy and decreases with increasing value of $E_{c.m.}$ in case of CF. This implies that a larger barrier modification is required at lower energies. However, at very high energies, the barrier modification becomes almost same. Therefore, drawing a connection between ΔV_B and ΔR, one may conclude that lower ΔR corresponds to higher barrier modification. Similar results are observed for ICF case in Fig.3.6(b) where magnitude of ΔV_B is much higher than CF process.

Furthermore, the cross sections addressed, using neck length parameter, are tabulated in Table 3.1 and 3.2, where the former one represents σ_{CF} and σ_{ICF} is shown in Table 3.2. It is clearly evident from Table 3.1 that the calculated complete fusion cross sections (including β_{2i}-deformed choice of fragmentation) find nice agreement with the experimental data. It may also be noted that the maximum angular momentum is almost same at all energies. Similar results are obtained for ICF expressed in Table 3.2. One important thing to mention here is that the energies in case of ICF have been obtained after applying the necessary energy corrections as per [2]. Hence, final beam energy in incomplete fusion is given as:

$$E_{beam}^{ICF} = E_{beam}^{projectile} - E_{beam}^{ejectile} \quad (6)$$

Table 3.1: *ER cross-sections calculated for $^{98}Tc^{*}$ nucleus formed in the CF reaction $^{9}Be + {}^{89}Y \rightarrow {}^{98}Tc^{*}$ using DCM at given center-of-mass energy range ($E_{c.m.}$=17.7-29.8MeV) analogous to the experimental data together with angular momentum and ΔR values.*

E_{lab}	$E_{c.m}$	T	ℓ_{max}	ΔR	σ^{DCM}	σ^{exp}
19.4	17.7	1.622	70	0.960	0.308	0.30±0.03
19.9	18.1	1.633	71	1.035	0.742	0.78±0.06
20.5	18.6	1.648	72	1.095	1.53	1.6±0.1
21.5	19.5	1.673	73	1.25	9.21	8.8±0.5
22.5	20.4	1.698	73	1.390	33.6	33.2±1.9
23.5	21.3	1.723	73	1.510	79.5	79.6±4.1
24.5	22.3	1.750	73	1.587	128	132±7
25.5	23.2	1.774	74	1.6	216	206±13
26.5	24.1	1.798	74	1.715	258	265±14
27.5	24.9	1.819	74	1.778	331	348±20
28.6	25.9	1.845	74	1.793	359	361±20
29.5	26.8	1.867	74	1.875	477.06	495±35
30.5	27.7	1.890	74	1.903	513	537±31
31.5	28.6	1.912	74	1.908	514	541±33
32.6	29.8	1.942	74	1.898	541	559±32

Table 3.2: *DCM based ER cross-sections calculated at center-of-mass energy range ($E_{c.m.}$=10.46-17.14MeV) for break-up channel $^{5}He+{}^{89}Y \rightarrow {}^{94}Nb^{*}$ analogous to the experimental data together with angular momentum and ΔR values.*

E_{lab}	$E_{c.m}$	T	ℓ_{max}	ΔR	σ^{DCM}	σ^{exp}
11.05	10.46	1.437	70	0.936	0.354	0.351
11.94	11.30	1.466	70	0.968	1.950	1.982
13.05	12.35	1.501	70	1.018	16.00	15.197
14.16	13.40	1.535	70	1.050	33.59	33.22
15.27	14.45	1.568	71	1.070	43.37	43.154
16.38	15.50	1.601	71	1.069	38.411	39.436
18.11	17.14	1.651	71	1.031	13.8	13.766

Further proceeding on with the comparative analysis of CF and ICF, the variation of barrier modification (ΔV_B) with respect to angular momentum ℓ, up to $\ell=\ell_{max}$, at three beam energies $E_{beam}(^{9}Be)$ 19.9MeV, 25.5 MeV and 32.6MeV is shown in Fig.3.7. At all these energies, the magnitude of ΔV_B decreases with increase in angular momentum i.e. larger barrier modification is needed at lower ℓ values as compared to higher ℓ values. Also, figure clearly depicts that the requirement of barrier modification is lesser in case of CF which is in accordance with the results obtained through Fig.3.6. Moreover, with increment in energy of incident beam, the difference between the magnitude of barrier modification for CF and ICF

keeps on rising resulting into the conclusion that very less amount of barrier modification is required for CF at higher incident energies.

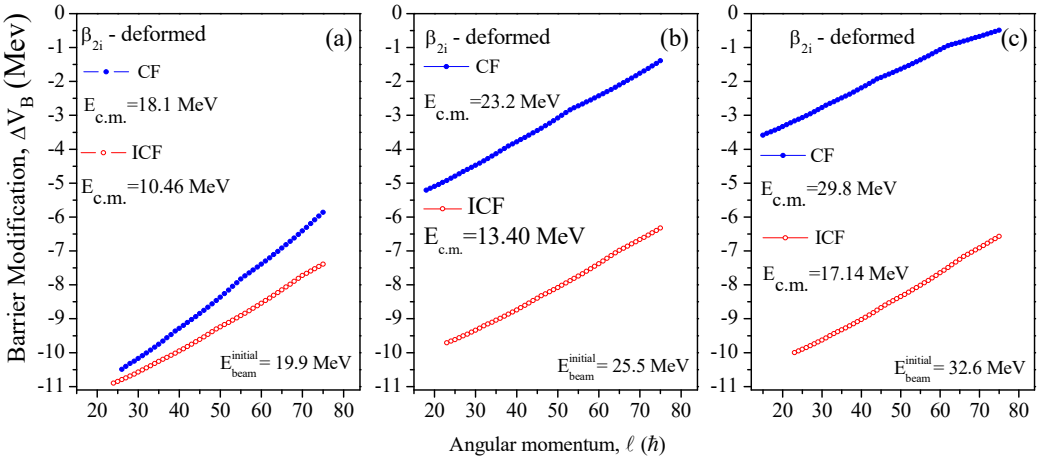

Fig.3.7. *Dependence of barrier lowering parameter ΔV_B on angular momentum (ℓ) at three different initial E_{beam}.*

The DCM calculated cross-sections (evaporation residue) for both the processes compared with the experimental data are shown in Fig.3.8. From the figure it is clearly visible that the DCM based ER cross sections are coherent with the available experimental data for both the processes. Besides this, the magnitude of cross-sections for CF process follow increasing trend with $E_{c.m.}$ However, in case of ICF, the same trend is not followed. The ICF cross sections are more dominant at energies near the barrier.

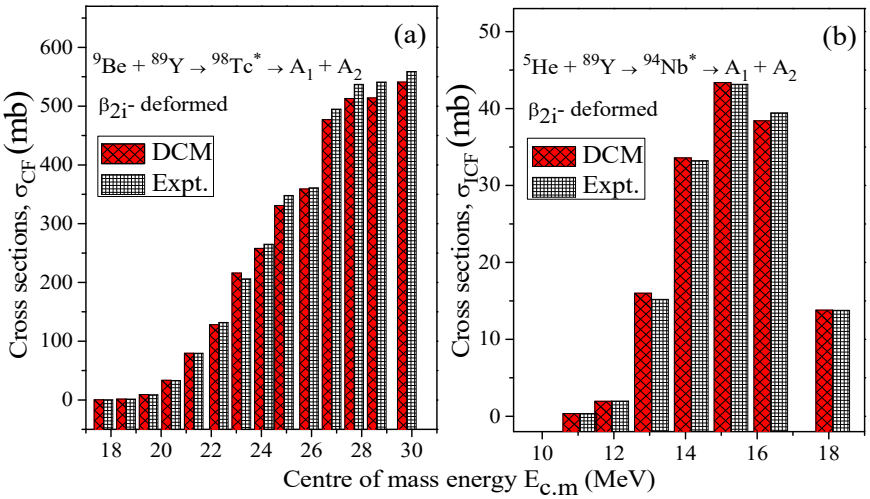

Fig.3.8. *Variation of (a) CF and (b) ICF cross sections with $E_{c.m.}$ compared with the experimental data.*

So far we have been interested in studying the nuclear reaction dynamics exhibited by weakly bound ^{9}Be induced reaction $^{9}Be + {}^{89}Y \rightarrow {}^{98}Tc^{*}$ where we examined the decay mechanism of the odd-proton and odd-neutron isotope of technetium (Tc) i.e. ^{98}Tc. Since, with the inclusion or exclusion of each nucleon, the properties of nucleus may alter vigorously, therefore the relative decay analysis of various isotopes of a nucleus is of huge importance.

On account of this, the decay of various isotopes of "Tc" has also been addressed by using weakly bound projectiles. The reason behind doing this isotopic study lies in the fact that the isotopes of technetium have various medical and industrial applications. The comparative analysis of decay paths has been done for $^{96, 98, 99, 100, 102, 104}$Tc isotopes at common excitation energy $E_{CN} \approx$ 37.9 MeV. From the available experimental data for the ER contribution for $^{96, 98, 102}$Tc isotopes in reference to [13], [2] and [12] respectively, calculations are carried out for the following reactions:

$$^{6}Li + {}^{90}Zr \rightarrow {}^{96}Tc^{*} \quad (6)$$

$$^{9}Be + {}^{89}Y \rightarrow {}^{98}Tc^{*} \quad (7)$$

$$^{6}Li + {}^{96}Zr \rightarrow {}^{102}Tc^{*} \quad (8)$$

Following the trend of the neck length parameter ΔR associated with above mentioned compound nucleus, the values of ΔR for neighboring isotopes are obtained through polynomial fitting, which may be verified in future experiments.

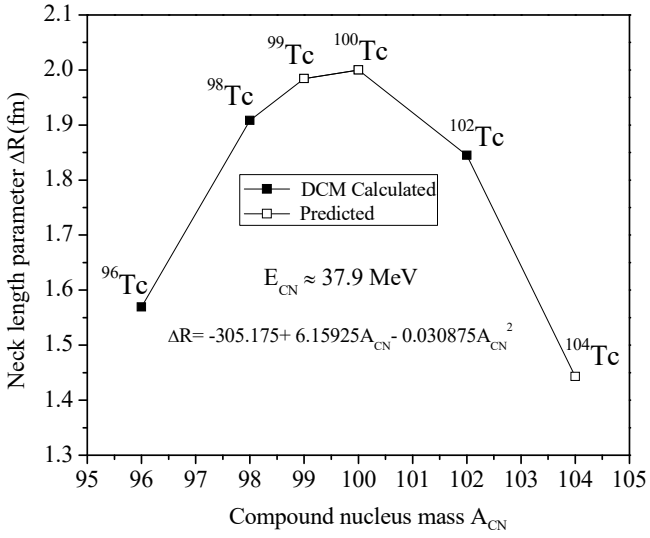

Fig.3.9. *Neck length parameter ΔR predicted for $^{99, 100, 104}Tc^{*}$ isotopes by using the calculated ΔR values at common excitation energy $E_{CN} \approx$ 37.9 MeV.*

Fig.3.9 illustrates the variation of ΔR for $^{96, 98, 99, 100, 102, 104}Tc^{*}$ isotopes at common excitation energy. The open symbols in figure represent the ΔR values for $^{99, 100, 104}Tc$ estimated through polynomial fitting (equation shown in figure) and the filled ones signify the fitted values of ΔR. Hence, the cross sections are obtained for neutron evaporation contribution by addressing various reaction channels as shown in Table 3.3. From this table, one can see that the cross-sections for $^{99, 100, 104}Tc$ are predicted using ^{6}Li and ^{9}Be induced reactions at same neck length parameter obtained through polynomial ($\Delta R = -305.175 + 6.15925A_{CN} - 0.030875A_{CN}^{2}$). Interestingly, for all three isotopes the cross-sections for ^{9}Be induced reaction lag behind the ones calculated via ^{6}Li induced reaction by 16-18 mb.

Table 3.3: *DCM based ER cross-sections calculated at common excitation energy $E_{CN} \approx 37.9$ MeV compared with the experimental data.*

Isotope	Incoming Channel	Temp.	ℓ_{max}	ΔR	σ^{DCM}	σ^{exp}
^{96}Tc	$^{6}Li + ^{90}Zr$	1.933	65	1.569	774	778±37
^{98}Tc	$^{9}Be + ^{89}Y$	1.912	74	1.908	514	541±33
^{99}Tc	$^{6}Li + ^{93}Zr$	1.902	75	1.984	384	Predicted
	$^{9}Be + ^{90}Y$	1.902	75	1.984	366	Predicted
^{100}Tc	$^{6}Li + ^{94}Zr$	1.892	65	2	324	Predicted
	$^{9}Be + ^{91}Y$	1.892	65	2	308	Predicted
^{102}Tc	$^{6}Li + ^{96}Zr$	1.871	71	1.845	745	752±47
^{104}Tc	$^{6}Li + ^{98}Zr$	1.855	70	1.443	286	Predicted
	$^{9}Be + ^{95}Y$	1.855	70	1.443	269	Predicted

Furthermore, the decay analysis of these isotopes of Tc is presented by showing preformation probability (P_0) as a function of fragment mass A_i (i=1, 2) in Fig.3.10 at similar excitation energy $E_{CN} \approx 37.9$ MeV. One can see that symmetric structure is obtained for lighter mass isotopes of Tc, however, as the compound nucleus mass increases, a triple humped structure starts arising in the fission region. It will be of further interest to evaluate fine structure effects in the decay pattern of Tc isotopes.

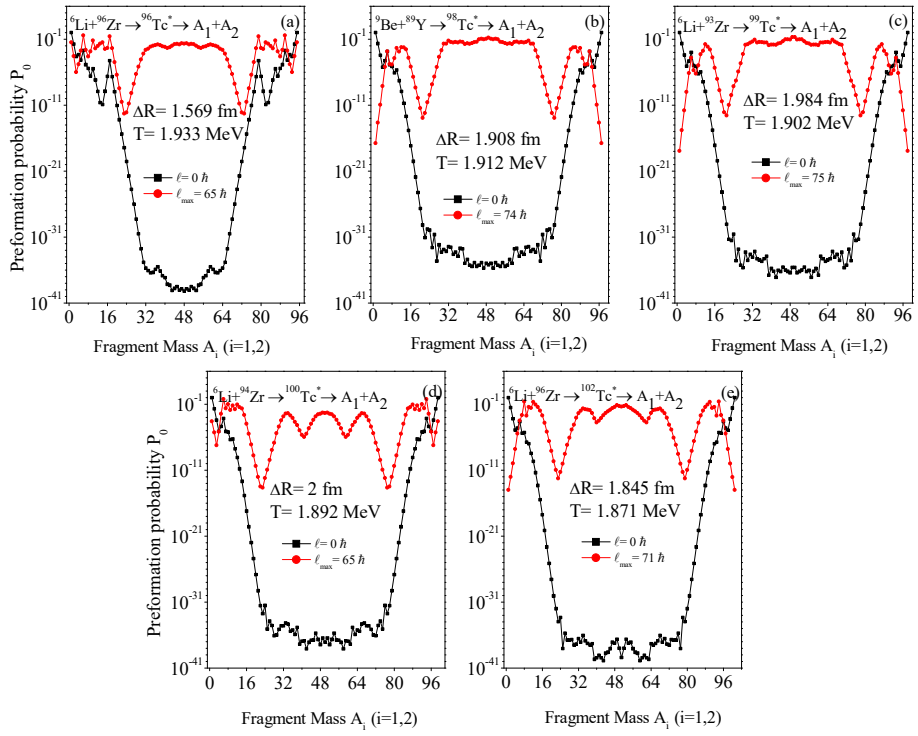

Fig.3.10. *Preformation probability (P_0) plotted as a function of fragment mass A_i (i = 1, 2) for the decay of different isotopes of Tc (a) $^{96}Tc^*$, (b) $^{98}Tc^*$, (c) $^{99}Tc^*$, (d) $^{100}Tc^*$, (e) $^{102}Tc^*$ and (f) $^{104}Tc^*$ at common excitation energy ($E_{CN} \approx 37.9$ MeV)*

References:

[1] L.F. Canto, P.R.S. Gomes, R. Donangelo, M.S. Hussein, Phys. Rep. **424**, 1 (2006).

[2]C. S. Palshetkar, S. Santraet al., Phys. Rev. C **82**, 044608 (2010).

[3] R.K. Gupta, M. Balasubramaniam,*et al.,*Phys.Rev. C **71**, 014601 (2005).

[4] R.K. Gupta, M. Balasubramaniam, R. Kumar, D. Singh, S. K. Arun and W. Greiner, J. Phys. G: Nucl. Part. Phys.**32**,345 (2006).

[5]G.Kaur, D. Jain, R. Kumar and M. K.Sharma, Nucl. PhysA**916**,260 (2013).

[6]G.Sawhney, G. Kaur, M. K. Sharma and R. K. Gupta, Phys. Rev. C **88**, 034603 (2013).

[7] M. Kaur and M. K. Sharma, Eur. Phys. J.A **50**, 61(2014).

[8] K. Sandhu. G. Kaur and M. K. Sharma, Nucl. Phys.A**21**, 114 (2014).

[9] S. K. Arun, R. Kumar and R. K. Gupta, Jour. Phys. G: **36**, 085105 (2009).

[10] M. Dasgupta, D. J. Hinde, R. D. Butt et al., Phys. Rev. Lett. **82**, 7 (1999).

[11] GurvinderKaur, Neha Grover, KirandeepSandhu, Manoj K. Sharma, Nucl. Phys. A **927,** 232(2014).

[12] S. P. Hu,G. L. Zhang,J. C. Yang et al., Phys. Rev. C **91**, 044619 (2015).

[13]H. Kumawat,V. Jha,V. V. Parkaret al., Phys. Rev. C **86**, 024607 (2012).

Summary:

The work done in this dissertation is particularly focused to address the dynamics of loosely bound induced reactions. Here, decay analysis of $^{9}Be+^{89}Y \rightarrow {}^{98}Tc^{*}$ reaction is carried out within the framework of DCM in which different possibilities for the break-up of ^{9}Be have been taken into account. Furthermore, an isotopic analysis of $^{96, 98, 99, 100, 102, 104}Tc^{*}$ has been done at common excitation energy (E_{CN}^{*}) addressing their respective decay paths. All the calculations have been performed for β_{2i}-deformed choice of fragmentation. The DCM calculated cross sections have been obtained by varying the neck-length parameter ΔR, and all these calculated cross sections have been found to be in nice agreement with the experimental data. The fragmentation potential and preformation probability for various reaction channels $^{5}He + {}^{89}Y \rightarrow {}^{94}Nb$, $^{4}He + {}^{89}Y \rightarrow {}^{93}Nb$ and $^{1}n+ {}^{89}Y\rightarrow {}^{90}Y$ for ICF suggests that neutron- induced ICF path is the least preferable of all whereas, the other two channels seem competing with each other. For better understanding of dynamics involved, the summed-up preformation probability as a function of angular momentum is plotted, which shows that ^{5}He induced reaction is the most dominant one followed by ^{4}He and neutron induced reactions. Further, the comparison of the decay paths resulting due to the complete and incomplete fusion processes suggests that, there is enhancement in probability of formation of IMFs in ICF channel. Also smaller neck is required for ICF which in turn demands higher barrier modification for ICF path. Besides this the role of angular momentum is also illustrated, which shows that larger barrier modification is needed at lower ℓ values as compared to higher ℓ states. The cross-sections follow increasing trend with increasing center-of-mass energy for CF whereas the ICF cross sections contribute most at near barrier energies. Finally, an isotopic analysis of $^{96, 98, 99, 100, 102, 104}Tc$ nuclei is carried out and the values of ΔR for $^{99, 100, 104}Tc^{*}$ are predicted using polynomial fitting, following the trend of ΔR of available data for neighboring isotopes ($^{96, 98, 102}Tc^{*}$). Consequently, cross sections are predicted for $^{99, 100, 104}Tc$ nucleus. The lighter isotopes of Tc show near symmetric fission distribution whereas a triple humped structure is seen for higher mass isotopes of Tc.